Measurement of the timing behaviour of off-the-shelf cameras

Volker Schatz

Fraunhofer IOSB, Gutleuthausstraße 1, 76275 Ettlingen, Germany

E-mail: volker.schatz∂iosb.fraunhofer.de

Abstract. This paper presents a measurement method suitable for investigating the timing properties of cameras. A single light source illuminates the camera detector starting with a varying defined delay after the camera trigger. Pixels from the recorded camera frames are summed up and normalised, and the resulting function is indicative of the overlap between illumination and exposure. This allows to infer the trigger delay and the exposure time with sub-microsecond accuracy. The method is therefore of interest when off-the-shelf cameras are used in reactive systems or synchronised with other cameras. It can supplement radiometric and geometric calibration methods for cameras in scientific use. A closer look at the measurement results reveals deviations from the ideal camera behaviour of constant sensitivity limited to the exposure interval. One of the industrial cameras investigated retains a small sensitivity long after the end of the nominal exposure interval. All three investigated cameras show non-linear variations of sensitivity at $\mathcal{O}(10^{-3})$ to $\mathcal{O}(10^{-2})$ during exposure. Due to its sign, the latter effect cannot be described by a sensitivity function depending on the time after triggering, but represents non-linear pixel characteristics.

PACS numbers: 85.60.Bt, 42.30.Va, 85.60.Gz

Keywords: Cameras, photodetectors, timing, calibration

Accepted by *Measurement Science and Technology*, IOP Publishing

DOI 10.1088/1361-6501/aa5d8a

1. Introduction

When using commercially available cameras for scientific purposes or evaluating their performance, it is common practice to perform a radiometric and geometric calibration. These methods serve to determine the spectral reponse and the geometric distortion, respectively. That allows to correct camera images before processing them further.

Cameras are frequently used in reactive systems acting on information from the camera image stream (e.g. [WCJ07]) and for measuring the movements of objects of interest (e.g. [FFI04, LC05]). However, there is no corresponding standard calibration procedure to determine the timing of a camera. Such a calibration method is particularly valuable when parameters such as a trigger delay are not specified by the manufacturer, when performing data fusion from multiple cameras (e.g. [WJV+04, Sch08]) or when the type of camera to use cannot be freely chosen because of conflicting requirements or because an existing system is to be investigated.

This paper presents a simple method that uses a single light-emitting diode (LED) to determine a potential delay and the sensitivity of a camera detector across its exposure interval. It works in principle as follows. The LED is controlled by the same timer that triggers the camera, with an adjustable delay. The pixel values from the resulting camera frames differ depending on the duration of illumination within the exposure interval and the sensitivity of the detector in that period. That allows inferring a trigger delay and the sensitivity at different points during exposure.

The following section describes the measurement setup in detail. Section 3 presents a theoretical model for camera exposure and formalises the idealised assumptions often made about a camera. Section 4 describes the course of a timing measurement. The methods used for analysing the data are described in section 5. Section 6 briefly presents prior work on camera timing and puts this paper into context. Experimental results for three cameras are presented in section 7. The last section will summarise the paper and discuss the scope for further research.

2. Experimental setup

The setup for camera timing measurements is quite different and in many ways simpler than for optical measurements. The camera is not used as an imaging sensor, so focus and alignment are no consideration. The cameras under investigation were in fact operated without any lens at all so that all pixels were illuminated equally and simultaneously. The camera detector was protected from dust by a transparent window. To prevent ambient light from degrading the measurements, the camera was attached to a closed box that also contained the light source, as shown in figure 1.

An LED was used as an illumination source, as LEDs react to changes in electrical current within the order of 10^{-7} seconds. The type of LED used was a Nichia NSPG520S, for which the switching times are documented [Nic03]. The rise time (time for switching on) is given as 62.46 ns, the fall time as 79.45 ns.

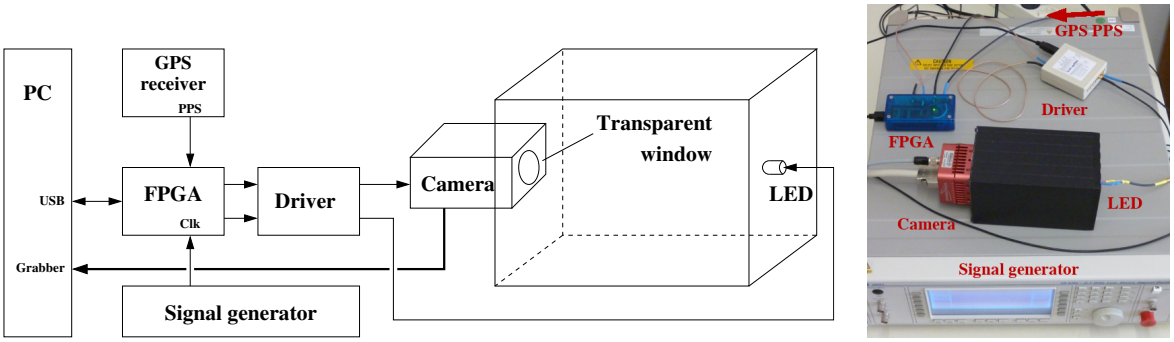

Figure 1. Measurement setup including trigger components. See text for a detailed explanation.

A trigger generator controlling the camera and the LED was implemented on a small Field Programmable Gate Array (FPGA) board attached to a PC via the USB bus. The board incorporates a Xilinx Spartan 3E FPGA, Flash RAM for the FPGA configuration and a microcontroller for interfacing with the USB bus[GOD09]. In order to allow the FPGA outputs to drive the LED and trigger the camera reliably, an additional line driver was added to the setup in a separate case.

The FPGA design contains two trigger generator circuits with adjustable period, pulse length and relative initial delay. The two trigger channels start operation with the given delay, and the trigger pulses will then drift relative to each other in proportion to their difference in frequency. The parameter registers and a control register that enables triggering can be accessed through short text commands via the USB bus.

The trigger generator was clocked by the 10 MHz frequency standard output of a signal generator of the type IFR 2041. In order to estimate time errors due to clock drift, the pulse-per-second (PPS) output from a Global Positioning System (GPS) receiver was fed into the FPGA. The FPGA circuit records a time stamp for each of those pulses, from which an error in the measured times was determined (see section 5).

The investigated cameras have Camera Link data interfaces and were read out with a frame grabber card in the PC. They were triggered via a separate general-purpose connector. They were operated in a trigger mode in which the exposure was determined by the trigger pulse width, so both trigger times and exposure and illumination durations were based on a common clock.

3. Idealised theoretical description

Before describing the measurement and analysis methods in detail, this section will develop the theory of the timing of an ideal camera. A result of the measurement method presented in this paper is the sensitivity of a camera detector over time during the integration of one frame. The function describing this sensitivity for a given pixel will be called the temporal response function R of that pixel and is defined so that the resulting pixel value is proportional to its cross-correlation with the incident light

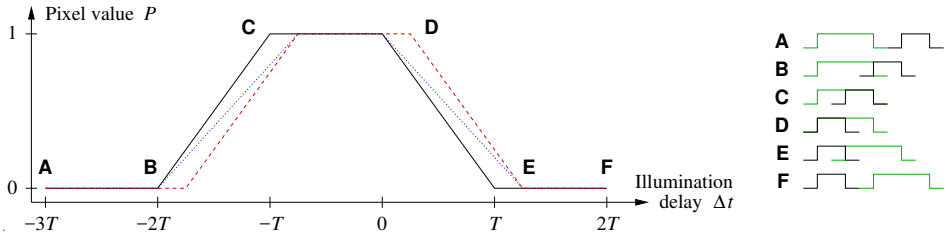

Figure 2. Normalised pixel values of an ideal detector illuminated for an interval of twice the exposure time T. The independent variable is the start of the illumination interval relative to the trigger time. The red dashed line applies if there is an internal trigger delay in the camera, the blue dotted line if the real exposure interval is longer than nominal (see text). The right part of the figure shows the relative timing of exposure (black) and illumination (green) for the six points marked in the graph.

intensity I:

$$P = \int_{-\infty}^{\infty} \mathrm{d}t \; R(t - t_{\mathrm{trigger}}) \; I(t) \tag{1}$$

Since R and I will not be measured in terms of physical units, they will be treated as dimensionless quantities. Furthermore, the LED providing the illumination can only be on or off, so we define I to assume only the values 0 and 1. R is normalised so that $P = 1$ for continuous illumination. This allows direct comparison with normalised measurement data.

The idealised temporal response function that is often assumed implicitly is a rectangular function with rising edge at time 0 whose width is the exposure time T:

$$R_{\mathrm{ideal},\,T}(t) = \frac{1}{T} \; B_T(t) = \frac{1}{T} \; \Theta(t) \; \Theta(T - t) \; , \tag{2}$$

where Θ is the Heaviside function and B_T is a box function of width T that will also be used in the following.

The LED illumination also has the form $B_T(t)$. The pixel value depends on Δt, the delay of the illumination start relative to the camera trigger. Denoting the illumination duration by T_I, the pixel value of an ideal camera is described by the following function:

$$P(\Delta t) = \int_{-\infty}^{\infty} \mathrm{d}t \; \frac{1}{T} \; B_T(t - t_{\mathrm{trigger}}) \; B_{T_I}(t - (t_{\mathrm{trigger}} + \Delta t)) \tag{3}$$

The result is a piecewise linear function, shown in figure 2 for $T_I = 2\,T$. The figure also displays modified curves for an internal trigger delay in the camera (red dashed line) and a deviating exposure (blue dotted line).

The case of an overlong exposure displayed by the blue dotted line requires some explanation. The slopes in the figure are the ranges of delays for which the illumination and exposure intervals overlap partially. Their width equals the exposure interval, making the slopes less steep for a longer exposure. The top plateau in the figure is the

range of delays where the illumination interval contains the exposure interval completely. This becomes shorter for a longer exposure time, giving a narrower plateau as shown in the figure.

All experimental results in this report pertain to cameras with a snapshot shutter that expose all pixels in a frame simultaneously. Therefore P and R apply to the detector as a whole rather than single pixels. Differences between pixels were not investigated, though the method would allow it.

Finally, it is worth noting a general relation that holds for any response function, provided the illumination function has the form $B_{T_I}(t)$ and T_I is larger than the support of the function R. Under those conditions, corresponding values in the rising and falling slopes of P add to 1:

$$\begin{aligned} P(\Delta t - T_I) + P(\Delta t) = & \int_{-\infty}^{\infty} \mathrm{d}t \; R(t - t_{\text{trigger}}) \cdot \\ & \cdot \left[B_{T_I}(t - (t_{\text{trigger}} + \Delta t - T_I)) + B_{T_I}(t - (t_{\text{trigger}} + \Delta t)) \right] \\ = & \int_{\Delta t - T_I}^{\Delta t + T_I} \mathrm{d}t' \; R(t') \;=\; 1 \quad \text{if} \;\; R(t') = 0 \;\; \forall \; t' \notin [\Delta t - T_I, \Delta t + T_I], \\ & \text{such as for} \;\; \Delta t \in [0,\; T_I], \quad R(t') = 0 \;\; \forall \; t' \notin [0,\; T_I] \,. \end{aligned} \tag{4}$$

The meaning of the last condition is that the illumination interval is large enough to cover the interval of sensitivity of the camera detector completely. This restriction was respected in all experimental measurements in section 7.

4. Triggering scheme and recording

The camera measurements presented below consist of sampling the curve in figure 2 from left to right. One such pass will in the following be called a sweep. The illumination interval was double the exposure time unless stated otherwise below. The initial illumination delay was negative enough that there was no overlap between exposure and illumination, as at point **A** in the figure. The camera trigger period was chosen smaller than that of the LED. Their difference is the increment by which the illumination delay increases between frames, i.e. the sampling interval on the Δt axis. The trigger periods and the exposure time were chosen to be integer multiples of that increment, so that the corner points **B** to **E** of the ideal sweep were hit exactly. This makes deviations at those points easy to detect.

Before investigating a camera, it was operated in the measurement setup with the LED always on. A maximum exposure time was determined so that no pixel value was saturated. This was done semi-automatically by bracketing the desired value between two guesses and refining it with successive interval subdivision. An exposure close to the resulting value (subject to divisibility by the desired sampling interval) was used in the timing measurements to minimise errors due to both saturation and noise.

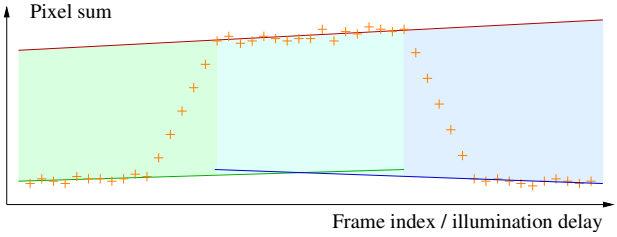

Figure 3. Schematic of a typical sweep measurement, with the drift in the plateaus exaggerated. Normalisation is performed between the high fit line and either one of the low fit lines (green and blue shaded regions) or an interpolation between both (cyan shaded region in the middle).

Camera frames were recorded using a data acquisition program accessing the frame grabber. This program is launched by a timing measurement master program which controls the trigger generator, starts and stops data acquisition and receives camera frames from the recording program. Data are analysed immediately as described in the following section, but frames are also recorded together with the trigger parameters to allow later inspection and reanalysis. Triggering is activated with a small delay after initiating data acquisition to make sure the first triggered frame is recorded and to maintain the correspondence between frames and illumination delays.

5. Analysis of pixel data

After recording a camera frame, the pixel data were processed for comparison with the theoretical curve. All cameras investigated for this report had a snapshot shutter exposing all pixels simultaneously. All pixels in each frame were summed up. Differences between individual pixels were not investigated, making the temporal response function R a property of the sensor as a whole. (By contrast, for rolling shutter cameras that expose different pixel rows at different times, the pixels in each row would have to be analysed separately.) When multiple sweeps were recorded, the pixel sums of frames corresponding to the same illumination delay were also added up. The resulting sums correspond one-to-one with the illumination delay Δt.

Some cameras show a slight drift in pixel sums while there is no or continuous illumination during exposure. This systematic effect was corrected for by normalisation with the help of straight lines fitted to the plateaus in a sweep as shown in figure 3. The most robust method of assigning measurement points to plateaus is based on sorting them by their ordinate value. The least-squares fit for the middle, high plateau is initialised by including the 10 highest points and the points between them. Then more data points to the left and right are added until a new point deviates from the existing fit by more than 5 standard deviations. Once the high plateau is identified and fitted, the lowest data points can be assigned to either the left or the right low plateau, and the same procedure is applied for fitting them.

Data points were then normalised by linear interpolation between the fit line of

one of the low plateaus (mapped to 0) and the line of the high plateau (mapped to 1). For the data points in the low plateaus and the slopes, the corresponding low fit line was used as a zero baseline; for the points in the high plateau the zero level was itself interpolated linearly between the two low fit lines. The errors of data points in the plateaus were determined as the RMS deviation from 0 (for the low plateaus) or 1 (for the high plateau). As the RMS deviation in the high plateau was more than an order of magnitude larger, the errors for slope points were interpolated between those in the adjacent plateaus. It is known that some types of noise in cameras increase with illumination [The95, IMUW08].

In the results presented below, multiple sweep measurements were combined by adding up pixel sums of the same illumination delay from each run. This incurs an error in the illumination delay in proportion to the clock drift between different runs. This error was estimated as the RMS deviation of the one-second intervals between successive time stamps of PPS pulses from a GPS receiver, which were recorded for that purpose. The time stamps from all the measurements presented in this paper were used to obtain a single error estimate, 43 ns, which was used in the analysis of all of them. The time stamps also allow to determine the systematic deviation of the clock frequency from the nominal. The relative deviation was $-1.33 \cdot 10^{-8}$, negligible compared to the errors of the numerical results.

6. Prior work

Work related to the timing properties of cameras and corresponding calibration methods is quite rare. The dated paper [HD65] presents light sources developed for the calibration of high-speed movie cameras. They are designed to be mounted inside the cameras and produce timing markers on the photographic film during recording. This precludes calibration after a recording has been completed, requires modifying the camera and is applicable only to cameras using photographic film.

Furthermore, the paper [BDL+97] may be considered prior work. It presents a camera system for investigating the propagation of the electrical potential in heart muscle tissue. It discusses temporal effects affecting such investigations, such as the changes in value of a given pixel in the presence of edges affected by motion blur. But no systematic investigation of the camera timing is made, and no method is suggested that could be used for that purpose.

A commercial LED array device [LED16] is intended for measuring the shutter release delay and exposure time of handheld photographic cameras. It is not intended for scientific use or for video cameras. The synchronisation with the shutter release button is mechanical, and the accuracy is given as “better than 1 ms”. The device works by switching the LEDs on successively and derives the shutter delay from which LEDs are lit in the recorded image. The method presented in this paper is simpler in that it uses only one LED and more accurate for several reasons: Both camera and LED are controlled electronically by the same clock, data from partial overlaps of illumination

Table 1. Measured trigger delays for the Basler avA1600-65km camera compared to delay register values. Errors apply to the last two decimals.

Trigger delay register value	Measured delay [μs] Rising / falling slope	
0	57.45±08	57.63±11
25 000	307.64±10	307.63±14
50 000	557.48±06	557.76±09
75 000	807.48±08	807.69±11
100 000	1057.58±09	1057.70±13

and exposure are analysed, and all pixels in a frame are used, reducing noise by orders of magnitude.

A method described in a recent set of patents [SI14, SI15] uses a LED array to display patterns instead of switching single LEDs. Successive patterns have a number of LEDs in common, which results in a brighter image and, according to the authors, increases accuracy by allowing a fast succession of patterns. Like the commercial LED array, that work is aimed at consumer photographic cameras and not intended for scientific use. The method of this paper is again both simpler and more accurate by comparison, for the same reasons as compared to the commercial LED array device. As the following section will show, it is also much more versatile than any previous method and allows investigating more complex camera properties than a trigger delay.

7. Experimental results

7.1. Trigger delays

For a first demonstration of the measurement method, a camera was chosen that allows setting an internal trigger delay, a Basler Aviator avA1600-65km. The camera detector was of Charge Coupled Device (CCD) type. The camera manual documents a 57 μs delay for activation of the frame trigger [Bas13]. The camera supports an additional trigger delay that can be adjusted by assigning a register value. According to the manual, the unit of the delay register value should be the camera time base, 1 μs, but the results below indicate otherwise.

A timing measurement was performed for delay register values from 0 to 100 000 in steps of 25 000. For each measurement, 10 sweeps of 501 frames were recorded with an exposure time of 0.7 ms.

The start of the slopes in the measured data was determined by computing the straight line through the first two slope data points and intersecting it with the plateau to the left of the slope. This method yields more accurate results than a linear fit to all slope data points for reasons that will be presented in section 7.3. The trigger delay is the difference between this slope start and the theoretical slope start.

Table 1 shows the results. The delays determined from rising and falling slopes are

displayed separately because they differ by several standard deviations. This difference may have physical causes: For points in the rising slope, the exposure interval starts while the sensor is being illuminated; in the falling slope, illumination starts during the exposure interval. These are different physical situations and can therefore have different delays.

A linear fit for the measured delays as a function of register values was performed using the scientific plotting program Gnuplot [Gnu] which uses the fit method presented in [Ore82]. It gives the following result, with error values applicable to the last two decimals:

$$t_{\text{delay, rising}} = (10.0004 \pm 11)\ \text{ns} \cdot n_{\text{Reg}} + (57.489 \pm 66)\ \mu\text{s}$$
$$t_{\text{delay, falling}} = (10.0008 \pm 08)\ \text{ns} \cdot n_{\text{Reg}} + (57.653 \pm 46)\ \mu\text{s}$$

The linear coefficients are in agreement within errors and show that the unit of the delay register is 10 ns, not 1 μs as documented in the manual.‡ The results for the overall additional delay differ by several standard deviations, but both support a value slightly larger than the 57 μs documented in the camera manual.

To determine the exposure time from the measured data, the end of each slope was determined analogously to the slope start. A straight line through the last two points of each slope was intersected with the following plateau. As shown in figure 2 and explained in the associated text, the width of the slopes is the camera exposure. The result does not differ significantly between different trigger delays and between the rising and falling slope. The overall average is (707.779$\pm$41) μs, 1.1% larger than the 0.7 ms width of the trigger pulse.

7.2. Post-exposure sensitivity of a CMOS detector

This investigation of a Photonfocus MV1-D1312-80-CL12 camera reveals the first deviation from the idealised view in section 3. Unlike the Basler camera from the previous section, this camera has a Complementary Metal Oxide Semiconductor (CMOS) detector. For reasons that will become clear, the length of the illumination interval was increased to eight times the exposure interval for this experiment. The exposure time was 4 ms, and 10 sweeps of 2503 frames each were recorded.

Figure 4 shows the high and right low plateaus of the result. The data contain curved parts after the linear slopes. That demonstrates that the camera's detector is still sensitive to illumination after the end of the nominal exposure interval. The brightness of recorded frames continues to increase until the illumination interval contains both the exposure interval and the post-exposure sensitivity region completely; and it does not reach zero until there is no overlap with the post-exposure region any more. The baseline of the right low plateau was fitted to the data in its right half only, and the baseline of the high plateau to its longest straight section, which was determined manually.

‡ This has been reported to the manufacturer, and the company has confirmed the result, which is due to a firmware bug.

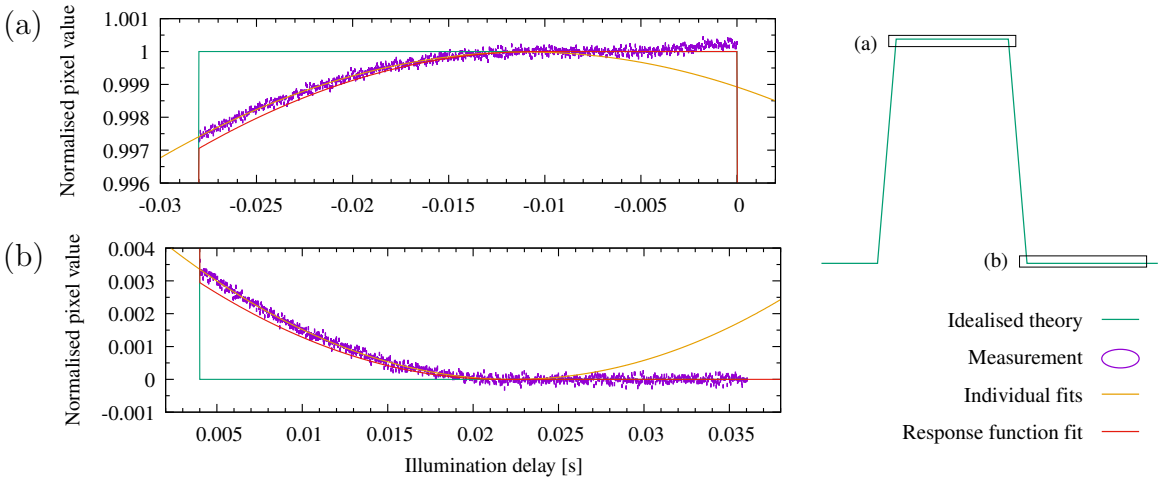

Figure 4. Sweep measurement data of the Photonfocus MV1-D1312-80-CL12 camera, demonstrating sensitivity after exposure. Part (a) of the figure shows the high plateau, part (b) the right low plateau, as indicated in the overview on the right. Data points are repesented by (very narrow) standard deviation ellipses. See text for an explanation of the fits.

The post-exposure effect is $\mathcal{O}(10^{-3})$ and differs slightly in size between the high and low plateau, i.e. depending on whether the sensor was illuminated during the exposure interval. The data are well fitted by parabolas:

$$\begin{aligned} P_{\text{postexp, high}}(\Delta\tau) &= (-8.86\pm22)\ \Delta\tau^2 - (0.1939\pm87)\ \Delta\tau + (0.998\,923\pm84) \\ P_{\text{postexp, low}}(\Delta\tau) &= (9.95\pm19)\ \Delta\tau^2 - (0.4451\pm49)\ \Delta\tau + (0.004\,973\pm28), \end{aligned} \tag{5}$$

where $\Delta\tau = \Delta t/1\text{s}$ is the illumination delay in seconds. The error values apply to the last two decimals. The fits are displayed in amber in figure 4.

If one disregards the differences between the two parabolas, the post-exposure sensitivity can be described by a modified temporal response function R. The illumination interval in the measurement was chosen large enough that the sensitivity was non-zero at only one of its endpoints at any time. Then, by (1), the rising slope of the normalised sweep is the derivative of R, and the falling slope is the negated derivative. The parabolic post-exposure part of the data gives rise to a decreasing linear part of R after the main box function component. The following ansatz was chosen, which is implicitly normalised:

$$R(\Delta t) = \begin{cases} R_0 & \text{for } 0 \le \Delta t < T' \\ 2\,\dfrac{1 - R_0\,T'}{(T'' - T')^2}\,(T'' - \Delta t) & \text{for } T' \le \Delta t \le T'' \\ 0 & \text{otherwise} \end{cases} \tag{6}$$

A simultaneous fit to the rising and falling slope and post-exposure data of the antiderivative of R yielded the parameter values:

$$R_0 = (249.24\pm17)\ \text{s}^{-1}$$

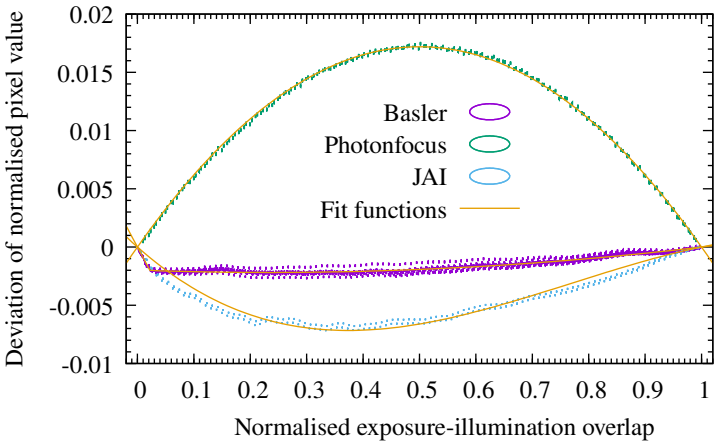

Figure 5. Deviation of slope data from linearity. Data points are represented by standard deviation ellipses. The independent variable is a normalised overlap between exposure and illumination. Data from the rising and falling slope of the sweeps, and from measurements with different delays for the Basler camera, were superimposed.

$$T' = (4.0004 \pm 35)\ \text{ms}$$
$$T'' = (21.6 \pm 3.9)\ \text{ms}$$

A temporal response function cannot be used to describe the difference between the after-exposure effects in the high plateau and the right low plateau. A given response function has the same effect in both places, but for mirroring with respect to the line $P = \frac{1}{2}$. The slight rise at the end of the high plateau (see figure 4 (a)) is also unexplained.

7.3. Exposure interval non-uniformity

A closer look at the data in the slopes of the sweep measurements reveals that they do not lie exactly on straight lines. This means that camera detectors do not have constant sensitivity during exposure. Furthermore, the deviation has the same sign in the rising and falling slope. Considering (4), this means they cannot be described by a temporal response function.

Figure 5 shows the deviation of slope data points from a linear slope for the two cameras from the previous sections and an additional CCD camera of type JAI CM-200 MCL. The data were obtained as follows. Straight lines through the first two and last two points of each slope, respectively, were intersected with the adjacent plateau at 0 or 1. This yielded slope start and end points without assuming linearity of the slope. The straight line through the start and end point of each slope was then used as a base line which was subtracted from the measured slope points. The independent variable was normalised to between 0 and 1 by looking up the base line value. This amounts to an illumination duration normalised as a fraction of the exposure interval.

The deviation from linearity is $\mathcal{O}(10^{-3})$ to $\mathcal{O}(10^{-2})$ depending on the camera. The data show small differences between measurement runs (Basler camera) and between rising and falling slopes (most easily visible for the JAI camera). The data of the

Photonfocus camera are symmetrical with respect to the point of 50% overlap. The data of the two CCD cameras are asymmetric, and their deviation from linearity is larger for smaller overlaps.

The Photonfocus camera data are very well described by a single-parameter fit of a parabola with zeros fixed at 0 and 1. The JAI camera data can be fitted with a third-order polynomial, with zeros at 0 and 1 fixed and two parameters remaining. The data of the Basler camera show a rather sharp kink on the left, which makes them hard to fit with a single smooth function. It was fit piecewise with a straight line for the steep step to the left and a parabola for the bulk of the data. The endpoints at 0 and 1 were fixed to zero as for the other fits, leaving three free parameters in total. The following parameters were determined:

$$\begin{aligned}
\Delta P_{\mathrm{Bas}}(p) &= \max \begin{cases} (-0.0907 \pm 18)\ p \\ (0.003725 \pm 58)\ (p-1)\ (p+0.532 \pm 13) \end{cases} \\
\Delta P_{\mathrm{Pf}}(p) &= (0.068785 \pm 60)\ p\ (1-p) \\
\Delta P_{\mathrm{JAI}}(p) &= (0.0326 \pm 10)\ p\ (1-p)\ (p-(1.311 \pm 26)),
\end{aligned} \tag{7}$$

where p is the normalised exposure-illumination overlap and the errors apply to the last two decimals.

7.4. Two cameras of the same type

While the previous sections have revealed differences between different types of cameras, comparing cameras of the same type can also be of interest. Some multi-camera systems are composed of cameras that are all of the same type [WJV+04], and a damaged camera will usually be replaced with the same type. This section presents results for a second Photonfocus camera of the same model as the one from section 7.2. The only difference is a slower data interface that causes a lower maximum frame rate, which is expressed in its full model designation MV1-D1312-40-CL-12. In the following it will be called the single-tap camera in contrast to the dual-tap camera from section 7.2, after the difference in interfaces.

The investigation of this camera was performed with exactly the same timing parameters as the one in section 7.2 to allow a one-to-one comparison. The LED was dimmed slightly with an additional resistor to prevent pixel value saturation.

While the behaviour of the single-tap camera is qualitatively similar to the dual-tap one, there are significant quantitative differences. The post-exposure effect differs in length and size, as shown in figure 6 for the right low plateau, corresponding to figure 4 (b). A parabola again provides a good fit, but with coefficients quite different from (5):

$$\begin{aligned}
P_{\mathrm{postexp,\ high}}(\Delta\tau) &= (-4.15 \pm 26)\ \Delta\tau^2 - (0.0714 \pm 98)\ \Delta\tau + (0.999\,698 \pm 89) \\
P_{\mathrm{postexp,\ low}}(\Delta\tau) &= (4.979 \pm 63)\ \Delta\tau^2 - (0.3699 \pm 26)\ \Delta\tau + (0.006\,855 \pm 23),
\end{aligned}$$

where $\Delta\tau = \Delta t/1\mathrm{s}$ is the illumination delay in seconds and the error values apply to the last two decimals.

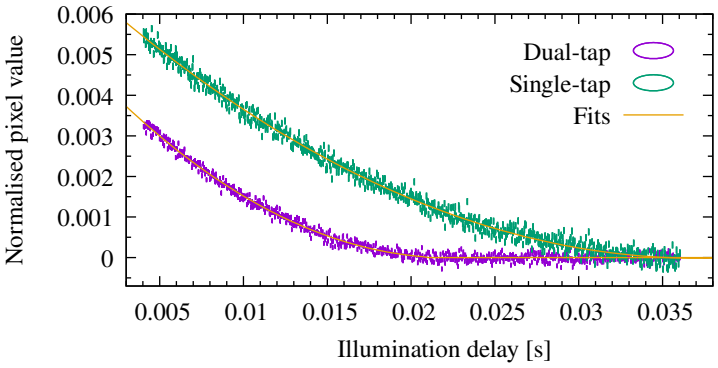

Figure 6. Comparison of the post-exposure effect in the right low plateau for two cameras of the type Photonfocus MV1-D1312 that differ only in the data interface. The Dual-tap camera is the same that was investigated in section 7.2. The post-exposure sensitivity of the single-tap camera extends significantly longer and differs in size.

The single-tap camera shows qualitatively the same deviation from a uniform exposure sensitivity, which is symmetric with respect to 50% overlap. The coefficient of the parabolic fit differs by a factor 0.77 from (7):

$$\Delta P_{\mathrm{Pf2}}(p) = (0.052982 \pm 65)\ p\ (1-p)$$

7.5. Discussion

The presented method, originally intended for determining a trigger delay, is suitable for investigating a much wider range of effects in imaging detector exposure. The CMOS cameras investigated exhibited declining but non-zero sensitivity for a duration far longer than the exposure time after the nominal end of exposure. For all cameras, average pixel values were not quite proportional to the intersection of the exposure interval with the illumination interval.

The latter effect cannot be described by a temporal response function as defined in (1). However, it is a function of the overlap between exposure and illumination. Therefore it is likely to be caused by a non-linearity in the accumulation of charge in the camera detector, and the fits (7) describe the non-linearities of the cameras' average pixel characteristics.

It is worth noting that the post-exposure sensitivity of the Photonfocus CMOS camera differed slightly depending on whether the start of exposure preceded the start of illumination or vice versa, and that this difference was consistent with the pixel non-linearity. The data are larger than the temporal response function (6) predicts, just as the data in the slopes exceed the linear theoretical values for this camera (see figure 4 and figure 5).

One last observation about the experimental results concerns the differences between the CMOS and CCD cameras investigated. The CCD cameras showed no post-exposure sensitivity. Their pixel characteristic non-linearities had the opposite

sign of those of the CMOS camera, and were asymmetric with respect to 50% overlap. Unfortunately only one type of CMOS camera was available for testing at the author's institution, so analysing systematic differences between camera detector technologies is outside the scope of this paper.

8. Summary and Outlook

This report has presented a measurement method that allows to determine a camera trigger delay and its exposure time with sub-microsecond accuracy. Triggering in a way that compensates these delays allows to synchronise different cameras' exposure to that same accuracy. This benefits work on data fusion from several cameras, which has previously relied on the tacit assumption that synchronisation is "good enough". The method could also be used to determine the inter-row delay of a rolling-shutter camera by analysing each pixel row separately. Considering the high accuracy of the full-frame results, a row-by-row analysis would still have acceptable accuracy despite reduced statistics.

This method also allows to go beyond the simple model implied in the designation of an exposure interval and to measure the course of a camera's sensitivity, the temporal response function. Experimental results from three cameras have shown that sensitivity during the nominal exposure interval varies by $\mathcal{O}(10^{-3})$ to $\mathcal{O}(10^{-2})$ depending on the camera. The single CMOS camera investigated shows a residual sensitivity for several exposure times after the nominal end of exposure. The latter effect appears not to have been investigated before. These results leave several questions open: By investigating more cameras, it could be decided if and how both effects depend on the camera detector technology, CMOS vs. CCD. For a specific camera, their dependence on exposure time and illumination brightness could be investigated. By varying the switching scheme of the LED, it could be verified that the exposure non-linearity permits an interpretation as an average pixel characteristic depending only on the amount of illumination.

On the whole, the contribution of this work is to show that camera exposure is not as simple a process as is often assumed and to provide the means to quantify it in detail. This allows to quantify the inaccuracies incurred in multi-sensor data fusion and other time-sensitive applications.

Acknowledgments

The author would like to thank Thomas Perschke for proof-reading the manuscript, and the anonymous referees for their suggestions and comments.

References

∼ confer ⇿ related ◁ background

[Bas13] ◁ Basler AG: Basler Aviator user's manual for Camera Link cameras. Oct 2013.

[BDL+97] ⇔ W. T. Baxter, J. M. Davidenko, L. M. Loew, J. P. Wuskell & J. Jalife: *Technical features of a CCD video camera system to record cardiac fluorescence data.* Annals of Biomedical Engineering **25** (1997) 713–725.

[FFI04] ◁ S. Funatani, N. Fujisawa & H. Ikeda: *Simultaneous measurement of temperature and velocity using two-colour LIF combined with PIV with a colour CCD camera and its application to the turbulent buoyant plume.* Measurement Science and Technology **15** (2004) 983–990. doi:10.1088/0957-0233/15/5/030.

[Gnu] ◁ *Gnuplot.* Http://www.gnuplot.info/.

[GOD09] ◁ OHO-Elektronik: GODIL User Manual. 2009. Online.

[HD65] ⇔ R. E. Hiller & L. M. Dearing: *Camera timing marker with dual spark and neon light sources.* Journal of the SMPTE **74** (1965) 897–901.

[IMUW08] ◁ K. Irie, A. E. McKinnon, K. Unsworth & I. M. Woodhead: *A model for measurement of noise in CCD digital-video cameras.* Measurement Science and Technology **19** (4) (2008) 045207. doi:10.1088/0957-0233/19/4/045207. Online.

[LC05] ◁ H.-Y. Lin & C.-H. Chang: *Automatic Speed Measurements of Spherical Objects Using an Off-the-Shelf Digital Camera.* In Proceedings of the 2005 IEEE International Conference on Mechatronics. 2005 .

[LED16] ∼ Image Engineering GmbH & Co. KG: LED-Panel V4. 2016. Online.

[Nic03] ◁ *Rise and fall time diagrams for Nichia NSP series LEDs.* Technical note. 2003. Online.

[Ore82] ◁ J. Orear: *Least squares when both variables have uncertainties.* American Journal of Physics **50** (1982) 912. doi:10.1119/1.12972.

[Sch08] ◁ V. Schatz: *Synchronised Data Acquisition for Sensor Data Fusion in Airborne Surveying.* In Proceedings of the 11th International Conference on Information Fusion (FUSION 2008). Jul 2008 pp. 1125–1130.

[SI14] ∼ R. Shiohara & T. Ichikawa: *Method, display device, and device for measuring shutter time lag.* International patent application. Apr 2014. WO 2014/057654 A1.

[SI15] ∼ R. Shiohara & T. Ichikawa: *Method, display device, and device for measuring shutter time lag.* European patent application. Aug 2015. EP 2908173 A1.

[The95] ◁ A. J. P. Theuwissen: Solid-state imaging with charge coupled devices. Kluwer Academic Publishing. 1995. ISBN 0-7923-3456-6.

[WCJ07] ◁ Y. Watanabe, A. J. Calise & E. N. Johnson: *Vision-Based Obstacle Avoidance for UAVs.* In AIAA Guidance, Navigation and Control Conference and Exhibit 2007. Aug 2007 AIAA 2007-6829.

[WJV+04] ◁ B. Wilburn, N. Joshi, V. Vaish, M. Levoy & M. Horowitz: *High-Speed Videography Using a Dense Camera Array.* In Proceedings of the 2004 IEEE Computer Society Conference on Computer Vision and Pattern Recognition, vol. 2. ISSN 1063-6919. 2004 pp. II–294–II–301. doi:10.1109/CVPR.2004.1315176.